Int. J. Heat Mass Transfer. Vol 21, pp. 1543–1553
Pergamon Press Ltd. 1978 Printed in Great Britain

THERMAL CONVECTION IN ROTATING SPHERICAL ANNULI—1. FORCED CONVECTION

R. W. DOUGLASS
Department of Mechanical Engineering, University of Nebraska, Lincoln, NE 68588, U.S.A.

B. R. MUNSON
Department of Engineering Science and Mechanics and Engineering Research Institute, Iowa State University, Ames, IA 50011, U.S.A.

and

E. J. SHAUGHNESSY
Department of Mechanical Engineering and Materials Science, Duke University, Durham, NC 27705, U.S.A.

(*Received* 17 *June* 1977 *and in revised form* 9 *March* 1978)

Abstract—The steady forced convection of a viscous fluid contained between two concentric spheres which are maintained at different temperatures and rotate about a common axis with different angular velocities is considered. Approximate solutions to the governing equations are obtained in terms of a regular perturbation solution valid for small Reynolds numbers and a modified Galerkin solution for moderate Reynolds numbers. The resulting flow pattern, temperature distribution, and heat-transfer characteristics are presented for the various cases considered. The theoretical heat-transfer results for small and moderate Reynolds number flows within a spherical annulus with a stationary outer sphere are compared with previous experimental results for the large Reynolds number flow situation. The difference between conduction, Stokes flow, and boundary-layer convection is shown.

NOMENCLATURE

c, specific heat;
$f(r)$, $g(r)$, $h(r)$, component functions for the approximate solutions;
N, truncation order for perturbation expansion;
N_T, truncation order for K–G expansion;
$P_m(\theta)$, Legendre polynomial of first kind and degree m;
Pr, Prandtl number $= \mu c/\kappa$;
$q(\theta)$, local wall heat-transfer rate;
Q, total heat-transfer rate;
r, radial coordinate;
R_1, R_2, inner and outer radius of the spheres;
Re, Reynolds number $= R_2^2\omega_0/\nu$;
$T(r,\theta)$, fluid temperature;
T_1, T_2, inner and outer temperature of the spheres;
$v(r,\theta)$, velocity component.

Greek symbols

α, perturbation solution coefficients;
$\zeta(r,\theta)$, dimensionless temperature function;
η, radius ratio, R_1/R_2;
θ, latitudinal coordinate;
κ, thermal conductivity;
μ, viscosity of the fluid;
$\tilde{\mu}$, angular velocity ratio, ω_2/ω_1;
ν, kinematic viscosity;
ϕ, longitudinal coordinate;
$\psi(r,\theta)$, stream function;
$\omega(r,\theta)$, angular velocity of the fluid;
ω_1, ω_2, angular velocity of the inner and outer spheres;
ω_0, reference angular velocity;
$\Omega(r,\theta)$, angular momentum function.

Subscripts

c, conduction;
m, n, order of component functions in perturbation solution;
n, order of component function in K–G solution;
r, θ, ϕ, vector components.

Superscripts

$\hat{}$, physical variable;
$'$, derivative with respect to r.

1. INTRODUCTION

WE PRESENT, in these companion papers, approximate solutions to the governing equations for steady convection in differentially rotating spherical annuli. This paper (Part 1) emphasizes convection in situations where buoyancy induced motions are very small. Part 2 discusses how these forced convection flows are modified by the presence of a uniform, radial body force field acting on a slightly compressible fluid. These results are intended to be general in nature and have a bearing on such studies as geophysical flows (Greenspan [1], Israeli and Orszag [2]) as well as providing insight into the study of secondary flows in rotating geometries.

Previous work concerning flow in spherical annuli can be grouped as either (i) isothermal rotating flows, (ii) heated non-rotating flows, or (iii) heated rotating flows. Many investigators have considered the isothermal flow (both spheres maintained at the same temperature) between two spheres rotating with different angular velocities. Among such theoretical studies are the low Reynolds number (Re) results of Haberman [3], Ovseenko [4], and Munson and Joseph [5]; the almost rigid rotation results of Proudman [6] and Stewartson [7]; and the numerical solutions of Pearson [8] and Greenspan [9]. Among the experimental isothermal spherical annulus flow studies are the basic flow results of Munson and Menguturk [10] and Sawatski and Zierep [11], and the stability results of Wimmer [12], Sorokin, Khlebutin and Shaidurov [13], and Yakushin [14]. Yavorskaya and Astaf'yeva [15] provide a recent review of works devoted to isothermal spherical annulus flow.

Several investigators have considered the stability of heated nonrotating spherical shell fluid layers—the spherical analog of the Bénard problem. Such investigations include those of Chandrasekhar [16], Joseph and Carmi [17], Busse [18], and Young [19].

Several studies concerning the combined natural and forced convection between rotating spheres have been carried out. These include the approximate boundary-layer solutions given by Singh [20] for a single sphere rotating in an infinite fluid and the low order perturbation solution given by Bentwich [21] for the same geometry. Experimental results for this geometry are given by Nordlie and Kreith [22] and Kreith, *et al.* [23]. Riley [24] and Riley and Mack [25] obtained a perturbation solution, valid for small Reynolds numbers, for the flow between two rotating spheres of unequal temperature with the gravitational field parallel to the axis of rotation. Experimental Nusselt number vs Reynolds number results for a rotating inner sphere and a stationary outer sphere of different temperatures were presented by Maples, *et al.* [26].

In this paper we consider the forced thermal convection in rotating spherical annuli for moderate values of Re in terms of a high order perturbation solution and a modified Galerkin procedure. The primary and secondary flow patterns, temperature distributions, and heat-transfer characteristics are presented for various parameter values.

2. GOVERNING EQUATIONS

The geometry for the spherical annulus flow considered is shown in Fig. 1. A viscous incompressible fluid fills the gap between the inner and outer spheres which are of radii R_1 and R_2, have uniform temperatures T_1 and T_2, and rotate about a common axis with constant angular velocities ω_1 and ω_2, respectively. Viscous dissipation is neglected and all fluid properties are assumed constant. Secondary flows in the meridian plane drive the forced convection.

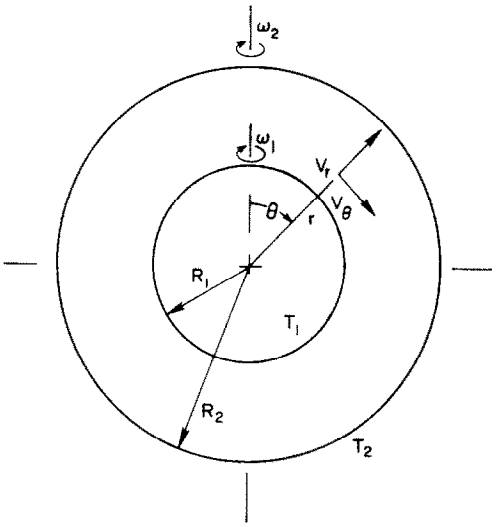

FIG. 1. The flow geometry.

Since the flow is assumed to be independent of the longitude, ϕ, the dimensionless Navier–Stokes equations and energy equation can be written in terms of a stream function in the meridian plane, ψ, an angular momentum function, Ω, and a temperature function, ζ, as follows (Douglass [27]):

$$\tilde{D}^2\Omega = \frac{Re}{r^2 \sin\theta} \cdot \frac{\partial(\Omega, \psi)}{\partial(r, \theta)}, \tag{1}$$

$$\tilde{D}^4\psi = \frac{Re}{r^2 \sin\theta}\left\{\frac{2}{r \sin\theta}\left[\Omega \frac{\partial(-r\sin\theta, \Omega)}{\partial(r, \theta)} + \tilde{D}^2\psi \frac{\partial(-r\sin\theta, \psi)}{\partial(r, \theta)}\right] + \frac{\partial(\tilde{D}^2\psi, \psi)}{\partial(r, \theta)}\right\}, \tag{2}$$

and

$$\nabla^2\zeta = \frac{RePr}{r^2 \sin\theta} \cdot \frac{\partial(\zeta, \psi)}{\partial(r, \theta)}, \tag{3}$$

where

$$\tilde{D}^2 = \partial^2/\partial r^2 + r^{-2}(\partial^2/\partial\theta^2 - \cot\theta\, \partial/\partial\theta),$$
$$\tilde{D}^4 = \tilde{D}^2(\tilde{D}^2),$$

and ∇^2 is the Laplacian operator in spherical coordinates. Jacobian notation for the derivatives has been used. For example,

$$\frac{\partial(A, B)}{\partial(r, \theta)} = \frac{\partial A}{\partial r}\frac{\partial B}{\partial \theta} - \frac{\partial A}{\partial \theta}\frac{\partial B}{\partial r}.$$

Various dimensionless groups arise from the nondimensionalization of the governing equations. The nondimensionalization employs R_2, ω_0^{-1}, and $(T_2 - T_1)$ as the characteristic length, time and temperature scales. Among the dimensionless groups are the radius ratio $\eta = R_1/R_2$, the angular velocity ratio $\tilde{\mu} = \omega_2/\omega_1$, the Reynolds number, and the Prandtl number. The Reynolds number is defined as $Re = \omega_0 R_2^2/\nu$. In general, $\omega_0 = \omega_2$, but if the outer sphere is stationary, then $\omega_0 = \omega_1$. The Prandtl number appearing in the energy equation (3) is $Pr = \mu c/\kappa$, where μ is the dynamic viscosity, c the

specific heat capacity of the fluid, and κ its thermal conductivity.

The flow is assumed to be symmetric with respect to the equator so that the range of independent variables is $\eta \leqslant r \leqslant 1$ and $0 \leqslant \theta \leqslant \pi/2$.

The actual physical variables are obtained from

$$\hat{v}_r = R_2\omega_0 \frac{\partial\psi/\partial\theta}{r^2\sin\theta}$$

$$\hat{v}_\theta = -R_2\omega_0 \frac{\partial\psi/\partial r}{r\sin\theta} \tag{4}$$

$$\hat{v}_\phi = R_2\omega_0 \frac{\Omega}{r\sin\theta}$$

$$\hat{T} = (T_2 - T_1)\zeta + T_1.$$

The angular velocity of the primary flow about the axis of rotation is given by $\hat{\omega} = \omega_0[\Omega/(r^2\sin^2\theta)]$, or in dimensionless form by $\omega = \Omega/(r^2\sin^2\theta)$.

The boundary conditions which complete the formulation of the problem are as follows:

$$\psi = \frac{\partial\psi}{\partial r} = 0 \quad \text{on} \quad r = \eta, \quad 1,$$

$$\zeta = 0 \quad \text{on} \quad r = \eta, \quad \zeta = 1 \quad \text{on} \quad r = 1$$

and either

$$\Omega = \eta^2\sin^2\theta \text{ on } r = \eta \text{ and } \Omega = \tilde{\mu}\sin^2\theta \text{ on } r = 1$$

if ω_1 is the characteristic angular velocity ($\omega_0 = \omega_1$) or

$$\Omega = \frac{\eta^2}{\tilde{\mu}}\sin^2\theta \text{ on } r = \eta \text{ and } \Omega = \sin^2\theta \text{ on } r = 1$$

if ω_2 is the characteristic angular velocity.

3. SOLUTION METHODS

Exact solutions of the equations governing the thermal convection in a rotating spherical annulus (equations 1–3) are as yet impossible to obtain. Solutions of these coupled, non-linear equations represent a wide variety of flow phenomena. It is possible, depending upon the values of the various parameters involved, to have any type of flow from creeping motion to boundary-layer flow (thermal and momentum). Two approximate methods of solution are used here to obtain laminar flow solutions. The first method is a regular perturbation technique valid for sufficiently small values of the Reynolds number. The second method is Kantorovich's modification of the well-known Galerkin technique, also known as a partial spectral expansion method. It provides solutions valid for Reynolds numbers larger than those of the perturbation technique.

As in the isothermal flow situation reported by Munson and Joseph [5], the small Re perturbation solution of equations (1)–(3) can be written in the form

$$\psi(r,\theta) = \sum_{n=0}^{N} Re^n \sum_{m=1,3,\ldots}^{n} g_{mn}(r)\sin^2\theta P_m(\theta),$$

$$\Omega(r,\theta) = \sum_{n=0}^{N} Re^n \sum_{m=0,2,\ldots}^{n} f_{mn}(r)\sin^2\theta P_m(\theta), \tag{6}$$

and

$$\zeta(r,\theta) = \sum_{n=0}^{N} Re^n \sum_{m=0,2,\ldots}^{n} h_{mn}(r)P_m(\theta),$$

where $P_m(\theta)$ is the mth-order Legendre polynomial of the first kind. The θ dependence of ψ, Ω, and ζ separates from the r dependence for this perturbation solution and allows the governing equations to be written as a system of linear, inhomogeneous ordinary differential equations for the component functions $f_{mn}(r)$, $g_{mn}(r)$, and $h_{mn}(r)$. Only N terms in the expansions are included, introducing the approximation to the exact solutions. N is equal to 4 for the results presented here.

These equations for the various component functions can be solved successively with the solution written in the following general form:

$$\Phi_{mn}(r) = \sum_{i,j} \alpha_{mn}^{ij} r^i (\ln r)^j. \tag{7}$$

Here, α represents an array of coefficients for the appropriate f, g, or h function. These coefficients are given in terms of the various parameters involved (η, $\tilde{\mu}$, and Pr).

Due to the uncoupling of the momentum and energy equations in forced convection flows, the f_{mn} and g_{mn} functions are the same for this forced convection problem as they are for the isothermal flow [5]. A detailed account of the solution method and a listing of the numerous α coefficients (through terms of order Re^4) can be found in Douglass [27]. It is noted that a solution consisting of f_{00}, g_{11}, and h_{00} represents a very small Reynolds number primary flow with its relatively small secondary flow and a conduction temperature profile, respectively. For larger Reynolds number flows, more terms in the expansion must be included in order to obtain valid solutions.

For still larger values of Re, an approximate solution of the governing equations can be obtained by a Kantorovich–Galerkin (K–G) method [28]. The dependent variables are expanded in a truncated series as follows:

$$\Omega(r,\theta) = \sum_{n=0}^{N_T} \sin^2\theta P_n(\theta) f_n(r),$$

$$\psi(r,\theta) = \sum_{n=0}^{N_T} \sin^2\theta P_n(\theta) g_n(r), \tag{8}$$

and

$$\zeta(r,\theta) = \sum_{n=0}^{N_T} P_n(\theta) h_n(r).$$

The non-linear ordinary differential equations governing the component functions $f_n(r)$, $g_n(r)$, and $h_n(r)$ are obtained by substituting this series representation for Ω, ψ, and ζ into the governing equations (1)–(3) and applying appropriate orthogonality conditions. The technique is similar to that used by Munson and Joseph [5] for the isothermal flow in a spherical annulus. Note that the expansion

utilizes Legendre polynomials as the eigenfunctions. This choice was made because of their "infinite" accuracy properties as shown by Orszag [29]. Note that here, N_T is 4. Details of the solution method may be found in Douglass [27] and are illustrated in Shaughnessy, *et al.* [30].

The solution to the resulting non-linear two-point boundary-value problem governing the component functions f_n, g_n, and h_n was obtained by numerical methods. A quasilinearization (or Newton–Raphson–Kantorovich iteration) method (Radbill and McCue [31]) proved to be quite acceptable. It is noted that the perturbation solutions described above are actually a solution of the linearized K–G equations. These perturbation solutions provide a convenient initial solution necessary to start the numerical iteration of the quasilinearization method.

The two approximate solution methods described above were used previously in determining the flow between two rotating spheres of equal temperature (Munson and Joseph [5]). It was found for this isothermal situation that solutions could be generated by the K–G method for Reynolds numbers considerably larger than obtainable by the perturbation method. For example, with $\eta = 0.5$ and $\tilde{\mu} = 0$, the K–G solution was found to remain valid for $Re \simeq 1000$ based on comparison of the K–G solution with previously reported finite difference solutions of the partial differential equations (Pearson [8]), whereas the high order perturbation solution was found to be valid only for $Re \leqslant 50$. Comparison of experimental results with the K–G solutions is also excellent (Munson and Menguturk [10]). It is not possible to compare our approximate forced convection solutions with previous finite difference solutions since none are available. Based on the above comments, however, we have no reason to doubt that for the range of parameters presented here ($Re \leqslant 200$, $Pr \leqslant 100$), the approximate solutions given are accurate.

4. DISCUSSION OF PERTURBATION SOLUTIONS

In this section we consider some of the properties of the steady forced convection flow of a viscous incompressible fluid in a spherical annulus. The solutions to the governing equations were obtained by the perturbation method discussed in the previous section.

If the bounding spherical surfaces were stationary, there would be no fluid motion and the temperature distribution would simply be the conduction distribution. Any rotation of the bounding spheres sets up a primary flow (ω) around the axis of rotation. If the spheres do not rotate at equal rates ($\tilde{\mu} \neq 1$), the relative motion sets up an unbalanced centrifugal force field which drives the secondary flows (ψ) in the meridian plane. Thus, if the bounding spheres are of unequal temperatures, this secondary flow produces forced convection within the annulus, resulting in a temperature distribution (ζ) that is different than

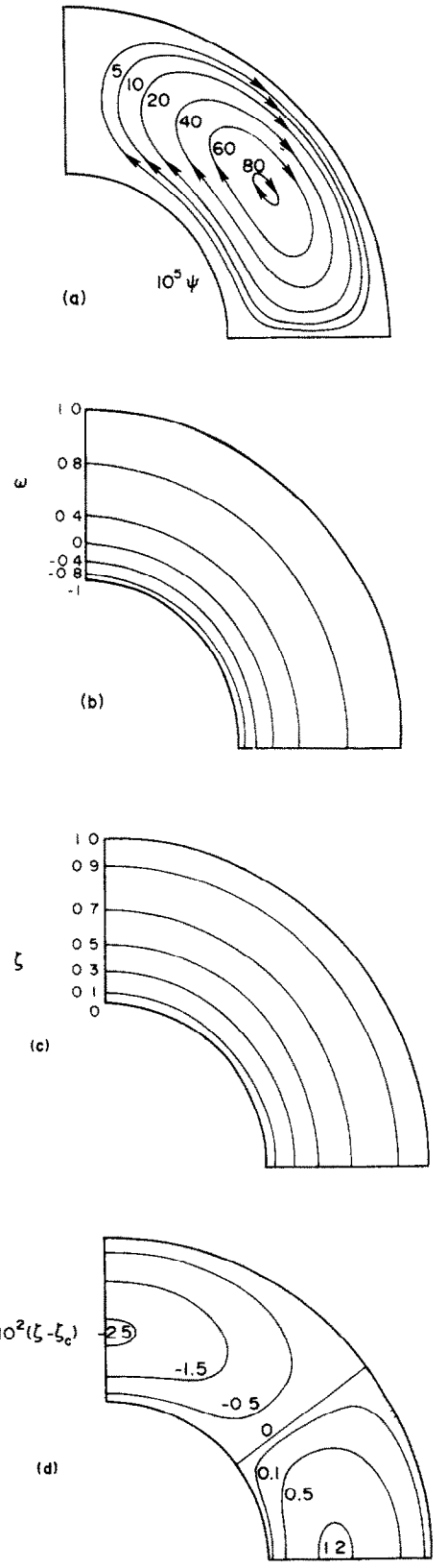

FIG. 2. Velocity and temperature distributions for $\tilde{\mu} = -1$, $\eta = 0.5$, $Re = \omega_2 R_2^2/\nu = 10$ and $Pr = 10$: (a) secondary flow; (b) primary flow and angular velocity; (c) temperature distribution; (d) difference between convective and conduction temperature distributions.

the pure conduction distribution. The relative magnitudes of the secondary flow and forced convection effects depend upon the parameters involved, including those concerning the geometry of the flow, η and $\tilde{\mu}$, and those concerning the dynamics, Re and Pr.

A typical situation is shown in Fig. 2 for the case when $\eta = 0.5$, $\tilde{\mu} = -1$, $Re = 10$, and $Pr = 10$. That is, the inner sphere has a diameter one half that of the outer sphere, and the spheres are rotating at the same angular velocity but in opposite directions. Terms through order Re^4 were included for this perturbation solution. It is seen that for $Re = 10$, inertial forces are not large. For example, the secondary flow in the meridian plane (Fig. 2a) is quite weak (maximum value of ψ is approximately 80×10^{-5}). The clockwise motion of the secondary flow indicates that the outer sphere is dominant as far as the secondary flow is concerned. The contours of constant angular velocity, ω (Fig. 2b), are nearly spherical shells. Hence, the secondary flow has not altered the primary flow to any noticeable degree. Likewise, the contours of constant temperature, ζ (Fig. 2c), are nearly spherical shells indicating that the secondary flow has caused only slight convective effects.

This effect of the secondary flow on the temperature distribution is shown by the $\zeta - \zeta_c$ contours of Fig. 2(d). Here ζ_c is the conduction temperature distribution, dependent only upon r. The difference between the actual and conduction distribution is dependent upon the magnitude of the secondary flow velocity (Re) and the rate of thermal diffusion (Pr). Consider the situation for which $T_2 > T_1$; that is, the outer sphere is hotter than the inner sphere. As shown in Fig. 2(a), the hot fluid near the outer sphere is convected toward the cooler inner sphere in the region near the equator, while the cool fluid near the inner sphere is convected toward the hotter outer sphere near the pole. Regions of warm and cool fluid then are formed in the equatorial and polar regions, respectively.

For relatively small values of Re and Pr, the forced convection temperature distribution is not greatly different than the conduction solution. For this case with $Re = 10$ and $Pr = 10$, the maximum difference is approximately 2.5%. From the perturbation solution, it can be shown that for small values of Re the difference between the convection and conduction temperature profile is proportional to Re^2Pr. For small Re, the "$\zeta - \zeta_c = 0$"-line separating the regions of ζ greater than or less than the conduction value is given by $P_2(\theta) = 0$, that is $\theta = 54.7°$.

The local rate of heat transfer across the bounding spherical surface is dependent upon the temperature gradient at the surface and may be written as

$$\hat{q} = -\kappa \frac{\partial \hat{T}}{\partial \hat{r}}. \tag{9}$$

This local heat flux may be put into dimensionless form by dividing the actual heat flux by the conduction heat flux value, $\hat{q}_c$, which is independent of θ. Use of the perturbation solution given by equation (6) results in the following heat-transfer ratio

$$\frac{\hat{q}(\theta)}{\hat{q}_c} = \left.\frac{\partial \zeta/\partial r}{\mathrm{d}\zeta_c/\mathrm{d}r}\right|_{r=\eta,1} = 1 + \frac{1}{h'_{00}(r)}\left[\sum_{m=2,4,\ldots}\sum_{p=0}^{m} Re^m P_p(\theta) h'_{pm}(r)\right]_{r=\eta,1} \tag{10}$$

where $r = \eta, 1$ denotes the value of the ratio at the inner or outer sphere, respectively. This local transfer ratio is a function of θ alone. The total heat transfer ratio, $\hat{Q}/\hat{Q}_c$, is obtained by integrating the local heat-transfer ratio over the surface of the bounding sphere. The resulting expression can be written as

$$\frac{\hat{Q}}{\hat{Q}_c} = 1 + \frac{1}{h'_{00}(r)}\left[\sum_{m=2,4,\ldots} Re^m h'_{0m}(r)\right]_{r=\eta,1}. \tag{11}$$

Here $\hat{Q}/\hat{Q}_c$ is the ratio of total heat transfer across the rotating spheres (forced convection) divided by that heat transfer for stationary spheres (conduction).

For small Re the local and total heat transfer ratios given above reduce to the following:

$$\frac{\hat{q}}{\hat{q}_c} = 1 + aRe^2Pr(3\cos^2\theta - 1) \tag{12}$$

and

$$\frac{\hat{Q}}{\hat{Q}_c} = 1 + ARe^4Pr^2, \tag{13}$$

where a and A are quantities dependent only upon η and $\tilde{\mu}$. Thus, the lowest order local heat-transfer convective effects are of the order Re^2Pr, whereas the total heat-transfer convection effects are of the order $(Re^2Pr)^2$. That is, when the θ-dependence of the local heat-transfer rate is integrated to form the total heat-transfer rate, the lowest order Re^2Pr term vanishes leaving the Re^4Pr^2 term as the lowest order correction to the total heat-transfer rate. These characteristics are also shown by the K–G solution and discussed in the next section. Values of $A(\eta, \tilde{\mu})$ are shown in Fig. 3 for two limiting cases; $\tilde{\mu} = 0$ and ∞. Since A is an index of the effect of convection on the total heat-transfer rate, this figure points out that $\eta \simeq 0.35$ is the optimum radius ratio. Further, the total heat-transfer rate drops off sharply for values of η approaching 0 or 1.

The Re^4 dependence of $\hat{Q}/\hat{Q}_c - 1$ shows that the forced convection effect for the overall heat-transfer rate is very small for small Reynolds number spherical annulus flows. That this is so is a result, in part, of the fact that the mechanism causing the forced convection is the secondary flow, which is relatively small for small Re. This is in contrast to a situation in which the primary flow is directly responsible for the forced convection. A heated sphere placed in a uniform stream of fluid is such an example. For this case it can be shown (Rimmer

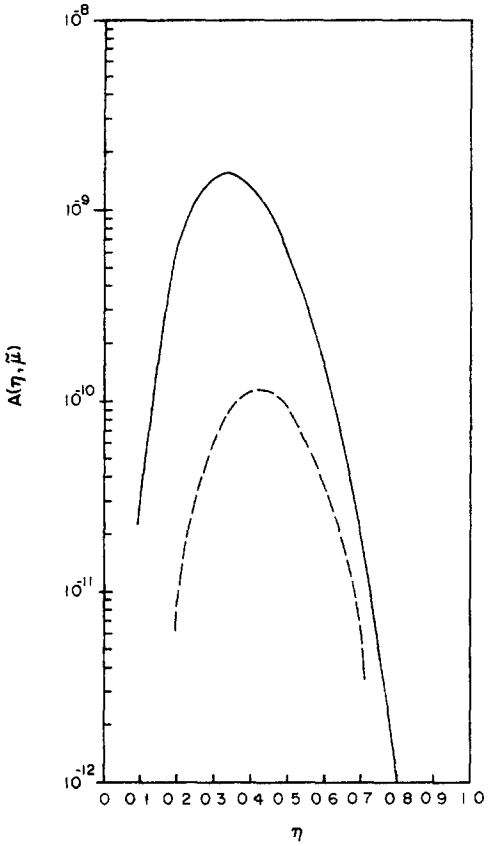

FIG. 3. The dependence of the total heat-transfer rate index on the radius and angular velocity ratios. (——) $\tilde{\mu} = \infty$, (----) $\tilde{\mu} = 0$.

[32]) that the lowest order correction to the total heat-transfer ratio is proportional to $RePr$.

5. DISCUSSION OF K–G SOLUTIONS

The K–G solution method discussed in Section 3 allows the forced convection solution to be obtained at Reynolds numbers larger than those permitted by the perturbation solution. For small Re, solutions obtained by the two methods agree to within several significant figures. In this section we discuss the solutions at larger Reynolds numbers than those allowed by the perturbation technique.

A typical situation is shown in Fig. 4 for the case where $\eta = 0.5$, $\tilde{\mu} = 0$ (the stationary outer sphere is twice the diameter of the inner one), $Re = 200$, and $Pr = 1$. Rotation of the inner sphere produces a centrifugal force field that drives the counterclockwise secondary flow as indicated in Fig. 4a. This outwardly centrifuging secondary flow near the equator interacts with the primary flow producing lines of constant angular velocity (Fig. 4b) that are different than the small Re, spherical shell structure. The shape of the constant temperature lines is likewise distorted from their spherical shell conduction condition as shown in Fig. 4(c). That these ω and ζ contours are very similar is not surprising since the distortion of each is dependent upon the relative amount of convection and conduction (thermal or momentum). For $Pr = 1$, the equations

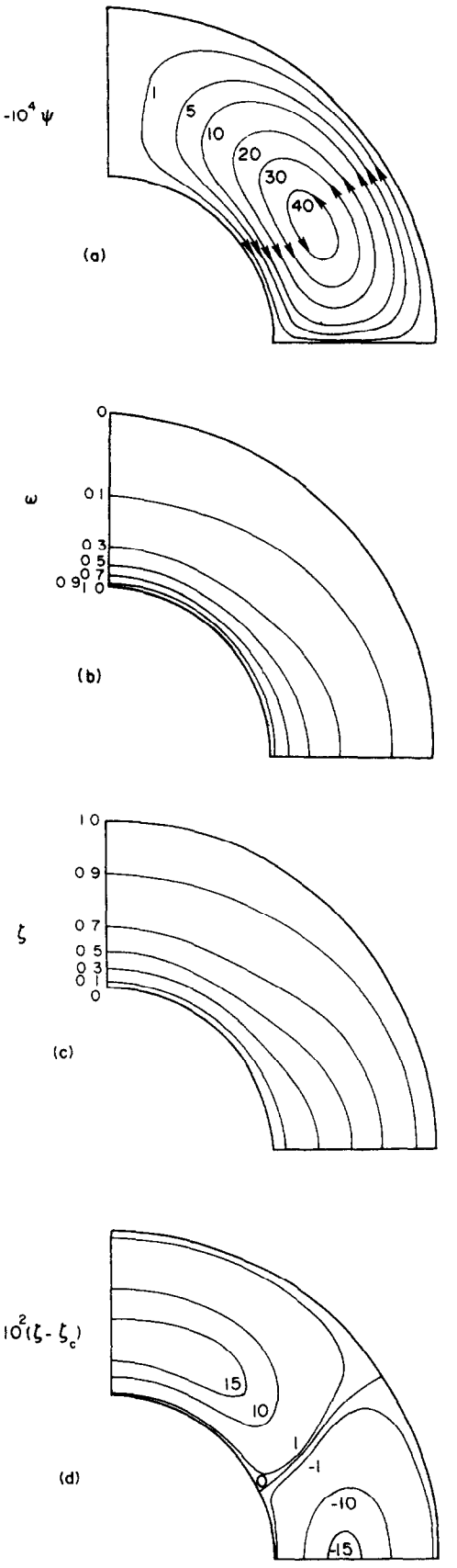

FIG. 4. Velocity and temperature distributions for $\tilde{\mu} = 0$, $\eta = 0.5$, $Re = \omega_1 R_2^2/\nu = 200$ and $Pr = 1$.

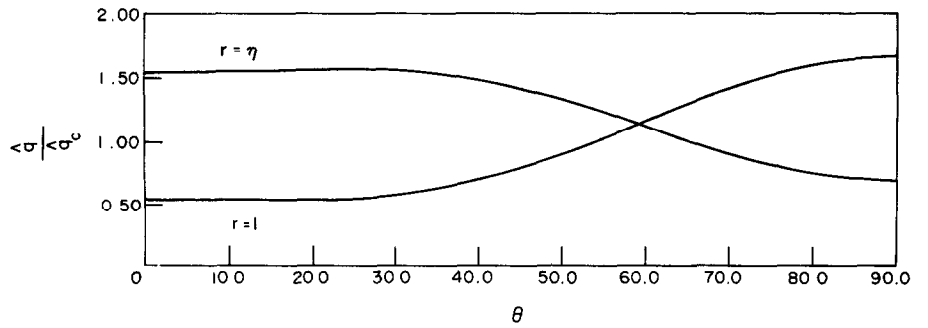

FIG. 5. Local heat transfer ratios at the spherical surfaces for $\tilde{\mu} = 0$, $\eta = 0.5$, $Re = \omega_1 R_2^2/\nu = 200$ and $Pr = 1$.

governing the basic flow momentum function (Ω) and the temperature function (ζ) are nearly identical. Recall that $\omega = \Omega/r^2 \sin^2\theta$. The difference between the convection and conduction temperature distributions, $\zeta - \zeta_c$, is shown in Fig. 4(d). The maximum difference is on the order of 15%. Thus, for example, if the outer sphere were hotter than the inner sphere, a region of relatively hot fluid is obtained in the region near the poles, while a region of relatively cool fluid is obtained near the equator. An equal but opposite effect is obtained for the situation where the inner sphere is hotter than the outer one. $(\zeta - \zeta_c)$ remains the same but $\hat{T} - \hat{T}_c$ changes sign [cf. equation (4)]. $\hat{T}_c$ is the dimensional conduction temperature distribution. For larger values of Re, the line separating these two regions is no longer a straight line as it was for the low order perturbation solution. The larger secondary flows produce stronger convective effects with more severe distortions of the temperature profile.

The heat-transfer characteristics of the larger Reynolds number K–G solutions can be obtained in a manner analogous to that described in the previous section for the perturbation solutions. In particular, the local and total heat-transfer ratios can be written as

$$\left.\frac{\hat{q}}{\hat{q}_c}\right|_{\eta,1} = \sum_{m=0,2,\ldots} P_m(\theta) \left.\frac{h'_m(r)}{h'_{00}(r)}\right|_{r=\eta,1} \tag{14}$$

and

$$\frac{\hat{Q}}{\hat{Q}_c} = \left.\frac{h'_0(r)}{h'_{00}(r)}\right|_{r=\eta,1} \tag{15}$$

where h_{00} is the conduction temperature function (from the perturbation solution). The local heat-transfer ratio for the flow shown in Fig. 4 and discussed above is shown in Fig. 5. As expected, the heat-transfer rate on the inner sphere ($r = \eta$) is maximum near the poles and minimum near the equator, whereas the opposite is true for the outer sphere. Thus, regardless of which sphere is hotter, the counterclockwise secondary flow causes the increased or decreased local heat-transfer rate as shown.

The overall heat-transfer rate, $\hat{Q}/\hat{Q}_c - 1$, is shown as a function of Reynolds number for $\tilde{\mu} = 0$ in Fig. 6. Results from the perturbation solution, the K–G solution, and experiments are shown. As discussed in

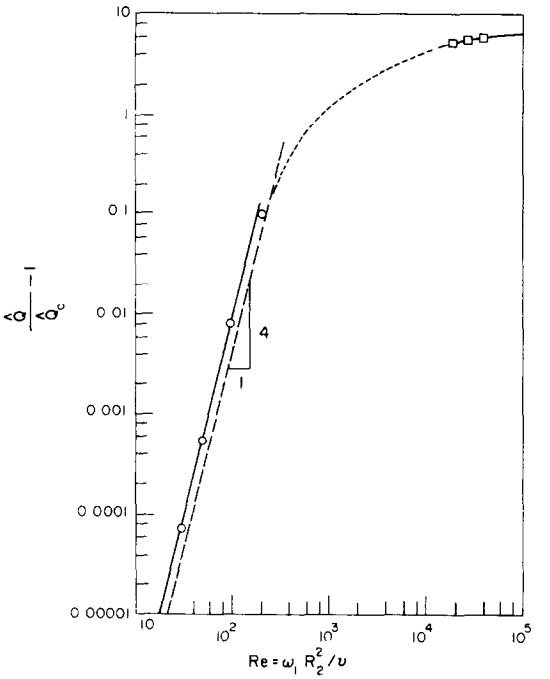

FIG. 6. Total heat-transfer ratio as a function of Reynolds number for $\tilde{\mu} = 0$, $\eta = 0.5$: — perturbation solution with $Pr = 1.0$; ○ K–G solution with $Pr = 1.0$; —— perturbation solution with $Pr = 0.72$; □ experimental results with negligible buoyancy and $Pr = 0.72$ (Maples, *et al.* [26]).

the previous section, for small Re the convection effects are of order Re^4. Hence, $\hat{Q}/\hat{Q}_c - 1$ becomes small very rapidly as the Reynolds number is decreased below $Re \simeq 100$ or so. The K–G solutions also show this type of Reynolds number dependence for small Re, while the dependence is not as strong for larger Re (see Fig. 6 for $Re = 200$).

The large Reynolds number experimental results of Maples, *et al.* [26] are shown on the same figure. These results were obtained by heat-transfer measurements within a spherical annulus with a stationary outer sphere ($\tilde{\mu} = 0$) oriented with the axis of rotation vertical. Hence, vertical buoyancy effects are present for the experiments but not for the theoretical results. However, for the data shown, the natural convection effects are very slight since the buoyancy parameter, Gr/Re^2 (where Gr is the Grashof number) is on the order of 0.33. The experimental results are for air with $Pr = 0.72$ rather

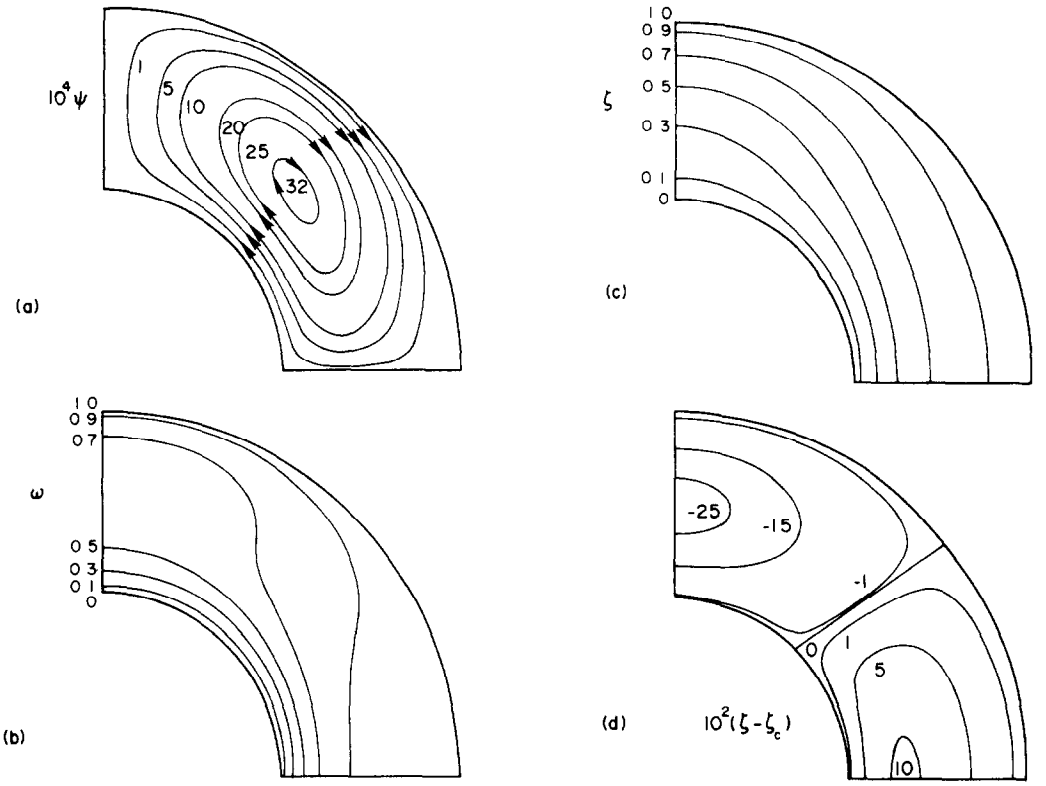

FIG. 7. Velocity and temperature distributions for $\tilde{\mu} = \infty$, $\eta = 0.5$, $Re = \omega_2 R_2^2/\nu = 200$ and $Pr = 1$.

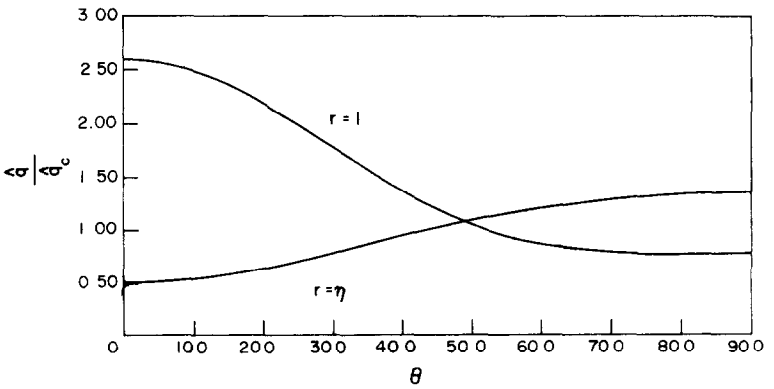

FIG. 8. Local heat-transfer ratios at the spherical surfaces for $\tilde{\mu} = \infty$, $\eta = 0.5$, $Re = \omega_2 R_2^2/\nu = 200$ and $Pr = 1$.

than $Pr = 1$ as calculated here. The theoretical low Re heat-transfer results for air are shown in the same figure.

The results for $\eta = 0.5$, $\tilde{\mu} = \infty$ (stationary inner sphere), $Re = 200$, and $Pr = 1$ are shown in Fig. 7. As reported previously ([5], [8], etc.), the centrifugal forces produce a clockwise secondary flow (Fig. 7a), and the angular velocity contours (Fig. 7b) show a typical cylindrical characteristic. That is, surfaces of constant ω are somewhat cylindrical in character as opposed to their low Re spherical character. Not surprisingly, the constant temperature contours (Fig. 7c) show a similar tendency toward a cylindrical characteristic.

As shown in Fig. 7(d), near the poles the difference between the forced convection and the conduction temperature distribution reaches a maximum of slightly more than 25%. This situation is similar to that in Fig. 4 and only here the regions of hot and cool fluid are interchanged. Again, the opposite effect is obtained if the inner sphere is hotter.

The local heat-transfer ratio on the bounding spheres is shown in Fig. 8. While the heat-transfer rate is not greatly different than the conduction value in the equatorial region ($45° \lesssim \theta \leqslant 90°$), it is considerably different in the polar region, particularly on the outer sphere. The total heat-transfer ratio is shown as a function of Reynolds number in Fig. 9.

As a final example, we consider the situation with $\eta = 0.5$, $\tilde{\mu} = -1/3$ (inner sphere rotating three times

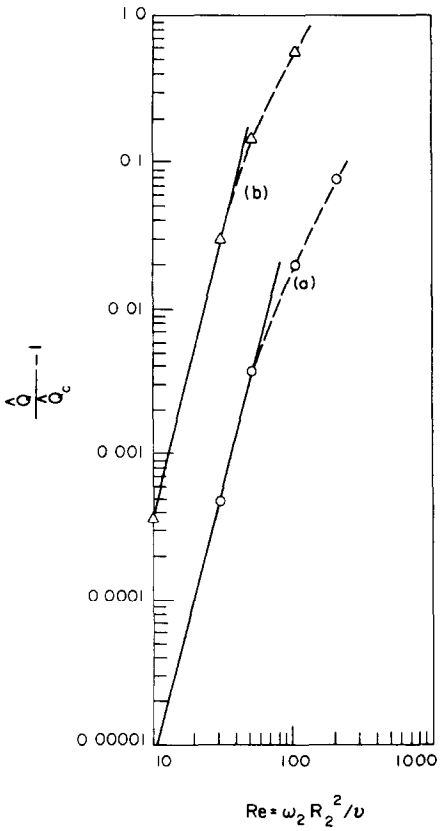

FIG. 9. Total heat-transfer ratio as a function of Reynolds number for $\eta = 0.5$: (a) $\tilde{\mu} = \infty$, $Pr = 1.0$, —— perturbation solution, ○ K–G solution; (b) $\tilde{\mu} = -\frac{1}{3}$, $Pr = 10.0$, —— perturbation solution, △ K–G solution.

that of the outer sphere and in the opposite direction), $Re = 50$, and $Pr = 10$. As shown in Fig. 10(a), neither of the spheres completely dominates the secondary flow. Two contrarotating swirls are obtained. Due to the relatively small Reynolds number, the contours of constant angular velocity (Fig. 10b) are essentially spherical surfaces. On the other hand, the relatively large Prandtl number causes a considerable distortion of the temperature profile (Fig. 10c). Surfaces of constant ζ remain quite spherical near the equator but are flattened considerably near the poles. Contours of constant $\zeta - \zeta_c$ are shown in Fig. 10(d). The total heat-transfer ratio results are included in Fig. 9. As the Reynolds number is increased, the deviation of the total heat-transfer ratio from the Re^4 low Reynolds number dependence is clearly demonstrated for both sets of data shown.

6. CONCLUSIONS

The forced convection within a rotating spherical annulus has been investigated by obtaining approximate solutions to the governing momentum and energy equations. The character of the velocity and temperature fields and the heat-transfer rates are strongly dependent upon the values of the various dimensionless parameters considered. For many cases the characteristics of the angular velocity and temperature distributions are quite similar. This is

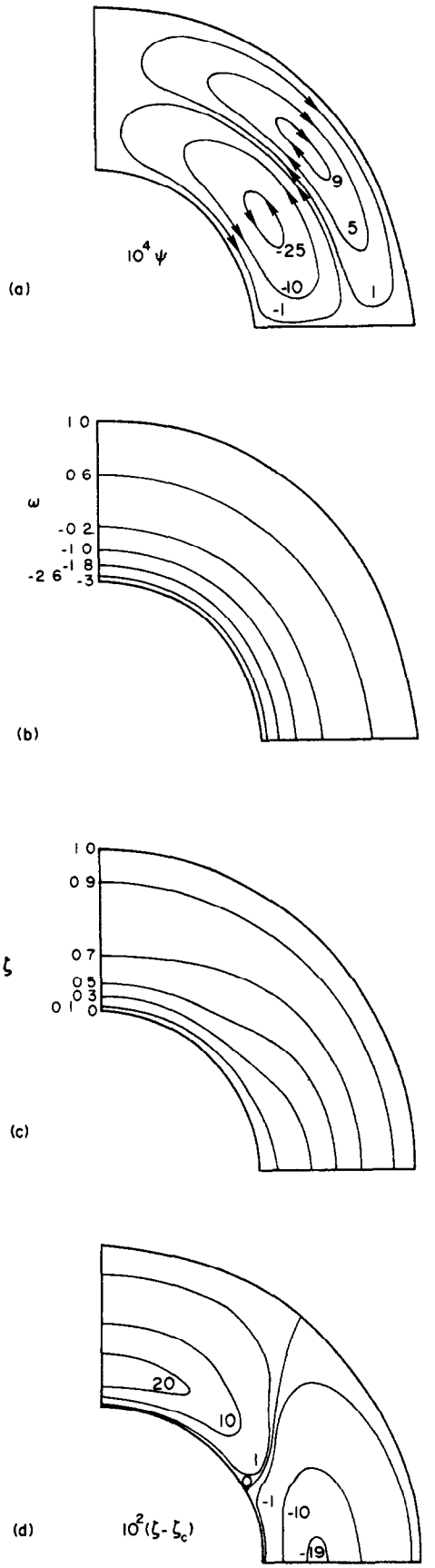

FIG. 10. Velocity and temperature distributions for $\tilde{\mu} = -\frac{1}{3}$, $\eta = 0.5$, $Re = \omega_2 R_2^2/\nu = 50$ and $Pr = 10$.

not unexpected since these distributions represent a balance between convection and conduction of momentum and heat, respectively. The results presented are for a radius ratio of one-half ($\eta = 0.5$). Similar characteristics are expected for other radius ratios, at least for values of η not too near zero or one.

The secondary flows that drive the forced convection become vanishingly small as $Re \to 0$. Thus, convective effects are quite weak for small Reynolds numbers, producing local heat-transfer ratios that do not differ considerably from the conduction value for small Re. This, coupled with the fact that on either sphere the local heat-transfer rate varies from greater than to less than the conduction value from the pole to the equator, results in an overall heat transfer rate that varies according to Re^4Pr^2 for small Re. For larger values of Re, this Reynolds number dependence becomes less severe.

Acknowledgement—The support by NSF Grant ENG7518398 and the Engineering Research Institute, Iowa State University, for portions of this work has been appreciated.

REFERENCES

1. H. Greenspan, *The Theory of Rotating Fluids*. Cambridge University Press, New York (1962).
2. M. Israeli and S. Orszag, Numerical investigation of viscous effects on trapped oscillations in a rotating fluid, in *Proceedings of the 5th International Conference on Numerical Methods in Fluid Dynamics*.
3. W. Haberman, Secondary flow about a sphere rotating in a viscous liquid inside a coaxially rotating spherical container, *Physics Fluids* **5**, 625–626 (1962).
4. Y. Ovseenko, On the movement of viscous liquids between two rotating spheres (in Russian), *Izv. Vyssh. Ucheb. Zaved., Matematika*, No. 4, 129–139 (1963).
5. B. Munson and D. Joseph, Viscous incompressible flow between concentric rotating spheres. Part 1: Basic flow, *J. Fluid Mech.* **49**, 289–303 (1971).
6. I. Proudman, The almost-rigid rotation of viscous fluid between concentric spheres, *J. Fluid Mech.* **1**, 505–516 (1956).
7. K. Stewartson, On almost rigid rotations—Part 2, *J. Fluid Mech.* **26**, 131–144 (1966).
8. C. Pearson, A numerical study of the time-dependent viscous flow between two rotating spheres, *J. Fluid Mech.* **28**, 323–336 (1967).
9. D. Greenspan, Numerical studies of steady, viscous flow between two rotating spheres, *Comput. Fluids* **3**, 69–82 (1975).
10. B. Munson and M. Menguturk, Viscous incompressible flow between concentric rotating spheres. Part 3: Linear stability, *J. Fluid Mech.* **69**, 705–719 (1975).
11. O. Sawatzki and J. Zierep, Flow between a fixed outer sphere and a concentric rotating inner sphere, *Acta Mechanica* **9**, 13–35 (1970).
12. M. Wimmer, Experiments on a viscous fluid flow between concentric rotating spheres, *J. Fluid Mech.* **78**, 317–336 (1976).
13. M. Sorokin, G. N. Khlebutin and G. F. Shaidurov, Study of the motion of a liquid between two rotating spherical surfaces, *J. Appl. Mech. Tech. Phys.* **6**. 73–74 (1966).
14. V. Yakushin, Instability of the motion of a liquid between two rotating spherical surfaces, *Fluid Dynamics* **5**, 660–667 (1973).
15. I. Yavorskaya and N. Astaf'yeva, Flow of viscous fluid in spherical layers (Review), NASA Technical translation: NASA TT F **16**, p.106 (January 1975).
16. S. Chandrasekhar, *Hydrodynamic and Hydromagnetic Stability*. Oxford University Press, New York (1961).
17. D. Joseph and S. Carmi, Subcritical convective instability. Part 2: Spherical shells, *J. Fluid Mech.* **26**, 769–777 (1966).
18. F. Busse, Pattern of convection in spherical shells, *J. Fluid Mech.*, **72**, 67–89 (1976).
19. R. Young, Finite-amplitude thermal convection in a spherical shell, *J. Fluid Mech.* **63**, 695–721 (1974).
20. S. Singh, Heat transfer by laminar flow from a rotating sphere, *Appl. Scient. Res.* **9**, 179–205 (1960).
21. M. Bentwich, The temperature distribution inside a rotating sphere and in the entire flow field around it. *Israel J. Technol.* **9**, 1–6 (*Proceedings of the 13th Israel Annual Conference on Aviation and Astronautics*, March 1971) (1971).
22. R. Nordlie and F. Kreith, Convective heat transfer from a rotating sphere, in *International Developments in Heat Transfer* (*Proceedings of the* 1961–62 *Heat Transfer Conference*), pp. 461–467 (1962).
23. F. Kreith, L. Roberts, J. Sullivan and S. Sinha, Convection heat transfer and flow phenomena of rotating spheres, *Int. J. Heat Mass Transfer* **6**, 881–895 (1963).
24. T. Riley, Thermal influence on the slow viscous flow of a fluid between rotating concentric spheres. Ph.D. Dissertation. University of Texas, Austin, Texas (1971).
25. T. Riley and L. Mack, Thermal effects on slow viscous flow between rotating concentric spheres, *Int. J. Nonlinear Mech.* **7**, 275–288 (1972).
26. G. Maples, D. Dyer, K. Askim and D. Maples, Convective heat transfer from a rotating inner sphere to a stationary outer sphere, *J. Heat Transfer* **95**, 546–547 (1973).
27. R. Douglass, Combined natural and forced thermal convection in a rotating spherical annulus, Ph.D. Dissertation, Duke University (1975).
28. L. V. Kantorovich and V. I. Krylov, *Approximate methods of Higher Analysis*. P. Noordhoff, Groningen, The Netherlands (1964).
29. S. Orszag, Numerical simulation of incompressible flows within simple boundaries. I. Galerkin (spectral) representations. *Stud. Appl. Math.*, **L**, 293–327 (1971).
30. E. Shaughnessy, J. Custer, and R. Douglass, Partial spectral expansions for problems in thermal convection, *J. Heat Transfer* **100**, 435–441 (1978).
31. J. Radbill and G. McCue, *Quasilinearization and Nonlinear Problems in Fluid and Orbital Mechanics*. Elsevier, New York (1970).
32. P. Rimmer, Heat transfer from a sphere in a stream of small Reynolds number, *J. Fluid Mech.* **32**, 1–7 (1968).

CONVECTION THERMIQUE DANS DES ESPACES ANNULAIRES SPHERIQUES—2. ECOULEMENTS STRATIFIES

Résumé—On considère la convection thermique mixte stationnaire d'un fluide de Boussinesq entre deux sphères concentriques. Les sphères sont maintenues à des températures différentes et tournent autour d'un axe commun avec des vitesses angulaires différentes. Un champ gravitationel, radial, uniforme agit sur le fluide. Des solutions approchées des équations sont obtenues par une méthode de Galerkin modifiée pour les nombres de Reynolds modérés. Les configurations d'écoulement, de distribution de température et les

caractéristiques de transfert thermique et de couple sont présentées pour plusieurs degrés de stratification. On constate que l'accroissement des forces de gravité altère les configurations d'écoulement primaire et secondaire aussi bien que les distributions de température. Les valeurs de transfert thermique et du couple sont augmentées en conséquence.

THERMISCHE KONVEKTION IN ROTIERENDEN KUGELFÖRMIGEN RINGRÄUMEN—I. ERZWUNGENE KONVEKTION

Zusammenfassung—Die stationäre erzwungene Konvektion in einer zwischen zwei konzentrischen Kugeln eingeschlossenen zähen Flüssigkeit wird untersucht. Die Kugeln werden auf unterschiedlichen Temperaturen gehalten und rotieren bei unterschiedlicher Winkelgeschwindigkeit um eine gemeinsame Achse. Für die maßgebenden Gleichungen wurden Näherungslösungen gefunden, und zwar für kleine Reynolds–Zahlen in Form einer Lösung mittels Störungsansatzes und für mäßige Reynolds–Zahlen in Form einer modifizierten Galerkin–Lösung. Für die verschiedenen betrachteten Fälle werden als Ergebnis das Stromlinienbild, die Temperaturverteilung und das Wärmeübertragungsverhalten dargestellt. Die theoretisch gewonnenen Wärmeübergangzahlen für Strömungen in einem kugelförmigen Ringraum bei kleinen und mittleren Reynolds–Zahlen und ruhender Außenkugel werden mit früheren Versuchsergebnissen für Strömungsverhältnisse bei großen Reynolds–Zahlen verglichen. Der Unterschied zwischen reiner Leitung, "Stokes–Strömung" und Grenzschicht–Konvektion wird gezeigt.

ТЕПЛОВАЯ КОНВЕКЦИЯ В ЗАЗОРЕ МЕЖДУ ВРАЩАЮЩИМИСЯ СФЕРАМИ. ЧАСТЬ I. ВЫНУЖДЕННАЯ КОНВЕКЦИЯ

Аннотация — Рассматривается стационарная вынужденная конвекция вязкой жидкости в зазоре между двумя концентрическими сферами, которые находятся при различных температурах и вращаются с различными угловыми скоростями вокруг общей оси. Получены приближенные решения исходных уравнений с помощью метода регулярных возмущений для малых значений числа Рейнольдса и посредством модифицированного метода Галёркина для средних значений числа Рейнольдса. Для рассматриваемых случаев приводятся картина течения, распределение температур и характеристики теплообмена. Для случая неподвижной внешней сферы теоретические результаты по теплообмену для течений, характеризующихся малыми и средними значениями числа Рейнольдса, сравниваются с ранее полученными экспериментальными данными для течений с большим числом Рейнольдса. Показано различие между режимами теплопроводности, стоксовского течения и конвекции в пограничном слое.